Rainbow metamaterials for broadband multi-frequency vibration attenuation: numerical analysis and experimental validation

H. Meng[1*], D. Chronopoulos[1], A. T. Fabro[2], W. Elmadih[3] and I. Maskery[4]

[1]*Institute for Aerospace Technology & The Composites Group, University of Nottingham, NG8 1BB, UK*

[2] *Department of Mechanical Engineering, University of Brasilia, 70910-900, Brazil*

[3]*Centre for Additive Manufacturing, Faculty of Engineering, University of Nottingham, NG8 1BB, UK*

[4]*Manufacturing Metrology Team, Faculty of Engineering, University of Nottingham, NG8 1BB, UK*

Abstract

In this study, we propose a 'rainbow' metamaterial to achieve broadband multi-frequency vibration attenuation. The rainbow metamaterial is constituted of a Π-shaped beam partitioned into substructures by parallel plates insertions with two attached cantilever-mass acting as local resonators. Both resonators inside each substructure can be non-symmetric such that the metamaterial can have multi-frequency bandgaps. Furthermore, these cantilever-mass resonators have a progressively variant design along the beam, namely rainbow-shaped, for the purpose of achieving broader energy stop bands. Π-shaped beams partitioned by parallel plate insertions can be extended to honeycomb sandwich composites, hence the proposed rainbow metamaterial can serve as a precursor for future honeycomb composites with superior vibration attenuation for more industrial applications. A mathematical model is first developed to estimate the frequency response functions of the metamaterial. Interaction forces between resonators and the backbone structure are calculated by solving the displacement of the cantilever-mass resonators. The plate insertions are modeled as attached masses with both their translational and rotational motion considered. Subsequently, the mathematical model is verified by comparison with experimental results. Metamaterials fabricated through an additive manufacturing technique are tested with a laser doppler receptance measuring system. After the validation of the mathematical model, a numerical study is conducted to explore the influences of the resonator spatial

* Corresponding author.
Email: han.meng@nottingham.ac.uk

distributions on the frequency response functions of structures. Results show that for metamaterials with both symmetric and non-symmetric resonators, rainbow-shaped resonators can introduce inertial forces inside wider frequency range when compared to the periodic resonators of the same total mass, hence broader bandgaps. Meanwhile, the attenuation inside the bandgaps decreases when the bandgap become broader. Metamaterials with broadband multi-frequency range vibration attenuation can be achieved with non-symmetric sinusoidally varying resonators.

Keywords: rainbow metamaterial, resonators, multi-frequency stop bands, broadband

1. Introduction

Metamaterials are a new class of artificial constructions consisting of microunits that are engineered to have novel properties. In the past decades, metamaterials have attracted tremendous attention from researchers in numerous research fields, thanks to the outstanding properties they manifest for manipulating waves in general.

Metamaterials were originally introduced for tailoring electromagnetic and optical waves [1-4]. Unusual properties such as negative magnetic permeability, electric permittivity and negative refractive index are achieved by electromagnetic metamaterials, which can be attributed to the resonance response of their metamolecules [1, 5]. The concept of metamaterials has been expanded to the elastoacoustic field in recent years. Such metamaterials are now widely applied in the fields of vibration and noise control [6-10], acoustic cloaking [11-13], seismic shields [14, 15], acoustic wave lensing [16, 17], wave trapping [18, 19] and acoustic black holes [20, 21] among other fields. Effective negative constants can be observed from elastic/acoustic metamaterials as well as electromagnetic metamaterials, including negative mass and dynamic stiffness [22-24], negative bulk modulus [25] and double negative characteristic [26, 27].

Another important feature of metamaterials is the existence of bandgaps, i.e. frequency bands within which no waves can propagate. These bandgaps are mainly generated by two phenomena, Bragg scattering and local resonances. Structures exhibiting Bragg destructive scattering are commonly known as phononic crystals. Bragg scattering bandgaps take place when the wavelength of travelling wave is comparable with the lattice dimensions of the metamaterial, consequently, it is hard to achieve in the low frequency range bandgap by phononic crystals. In contrast, locally resonant bandgaps rely on the resonance of internal oscillating inclusions. The local resonance bandgaps occur at frequencies much lower than Bragg scattering ones and are associated with the imaginary part of the unity cell propagation constant, i.e., rapidly decaying waves, instead of negative group velocity as it is usually misunderstood. Liu *et al*. [28] first fabricated an elastic metamaterial by periodic inclusions coated with soft rubber. The proposed elastic metamaterials exhibited bandgaps at frequencies where the lattice dimensions are two orders of magnitude smaller than the wavelength. Henceforth, more metamaterial designs have been proposed with various local resonators, including Helmholtz resonators [7, 25], cantilever beam oscillators [29] and membrane members with attached masses [30, 31], rubber rings surrounded by metal rings [32], and so forth. These local resonators are combined with engineering structures such as rods, beams and plates to constitute elastic/acoustic metamaterials for low frequency vibration suppression. For instance, Nobrega *et al*. [33] and Xiao *et*

al. [34] investigated bandgaps of metamaterial rods combined with periodically attached local resonators through a Finite Element (FE) approach. Huang *et al*. [35], Zhang *et al*. [31] and Yu *et al*. [36] proposed metamaterials dedicated to flexural wave bandgaps and attenuation by combining engineering beams with various local resonators. Xiao *et al*. [37] and Li *et al*. [38] presented plate-type metamaterials consisting of plates with out-of-plane local resonators, i.e., the local resonators are attached or deposited to the surfaces of plates. Nouh *et al.* [39] developed metamaterials with plates and built-in local resonators. The abovementioned locally resonant metamaterials consist of different engineering structures and local resonators, but most of them contain one resonator in each periodic unit, hence have a single resonance bandgap at low frequencies. A few researchers proposed metamaterials with multiple resonators which had multi bandgaps. Instead of a single resonator, two or more integrated resonators exist in each unit cell of these metamaterials. Huang and Sun [40], Chen *et al*. [41] created two resonator mass-in-mass lattice structures that had multiple bandgaps. Pai *et al.* [42], Peng *et al.* [43], Xiao *et al.* [44], and Miranda Jr *et al*. [45] proposed multi stopband metamaterials by replacing single mass-spring resonators with two integrated mass-spring subsystems.

Even though locally resonant metamaterials are capable of manipulating wave propagation and provide effective vibration attention, their narrow bandgaps limit their applications for industrial purposes. The design of metamaterials with broad bandgaps remains a critical and challenging topic for researchers in related areas. Metamaterials with spatially varying resonators came into the view by few researchers. Sun *et al.* [46] and Pai [47] made the first attempt at developing elastic metamaterials with spatially varying mass-spring-damper subsystems. Their investigations showed the prospect of enlarging the bandgap with properly designed spatially varying local resonators. Nonetheless, as far as we know, no relevant research has been found on the influence of nonperiodic resonators systematically, let alone proposed metamaterials with well-designed spatially varying resonators.

In this manuscript, we present for the first time a systematic study for metamaterial with rainbow-shaped resonators that aim at enlarging local resonance bandgaps. The proposed metamaterial includes linearly varying or sinusoidally varying cantilever-mass resonator in the substructure of the Π-shaped beams partitioned by plate insertions. Frequency response functions (FRFs) of the rainbow metamaterial are estimated by the new mathematical model concerning the dynamics of cantilever-mass structures and transfer matrix between segments of the rainbow metamaterial. Compared with conventional FE model that requires large computation time and computer memory, the mathematical model can give efficient prediction of dynamic properties of rainbow

metamaterials, hence is more applicable for exploring design routes or conducting further optimization for the rainbow metamaterials. Experimental results are also offered validating the exhibited analytical scheme. The influence of rainbow resonators is studied and design suggestions are given through a numerical parametric study.

This paper is structured as follows. Section 2 gives a description of the rainbow metamaterial. A mathematical model is proposed to estimate the FRFs of the proposed metamaterial efficiently. Subsequently, the mathematical model is verified in Section 3 by comparison with experimental results. An additional numerical study is conducted in Section 4 to investigate the influence of non-symmetric rainbow-shaped resonators. Finally, Section 5 draws some concluding remarks and further perspectives.

2. Mathematical modelling method for the structural dynamics of the rainbow metamaterial

A mathematical modelling method is set up in this section to determine the structural dynamics of the rainbow metamaterial. Figure 1 shows the schematic of the proposed rainbow metamaterial. The Π-shaped beam is partitioned into substructures by periodic plate insertions. Non-symmetric cantilever-mass subsystems are clamped to the two side walls of the Π-shaped beam in each substructure. Instead of being periodic, the resonating subsystems are spatially varying along the length of the beam. The interaction forces between the Π-shaped beam and cantilever-mass resonators as shown in Fig. 2 are initially derived. Subsequently, the displacement transfer matrix and FRFs of the rainbow metamaterial are deduced.

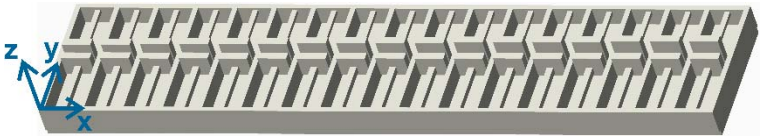

Fig. 1 Schematic of the rainbow metamaterial with non-symmetric spatially varying resonators.

2.1 Interaction force between Π-shaped beam and cantilever-mass resonators

The interaction force between the Π-shaped beam unit cell and two non-symmetric local resonators, described in terms of the vibration of a single cantilever-mass resonator (see Fig. 3), is analyzed first.

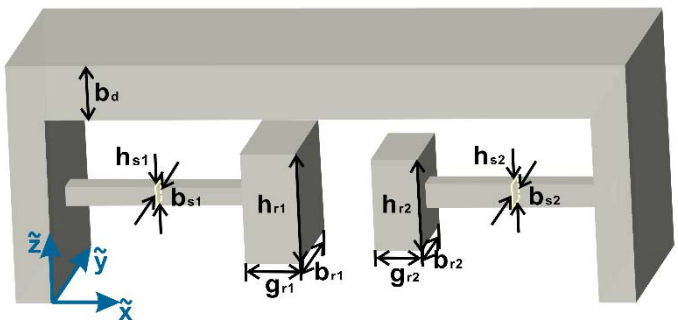

Fig. 2 Schematic diagram of the unit cell of Π-shaped beam with non-symmetric cantilever -mass resonators.

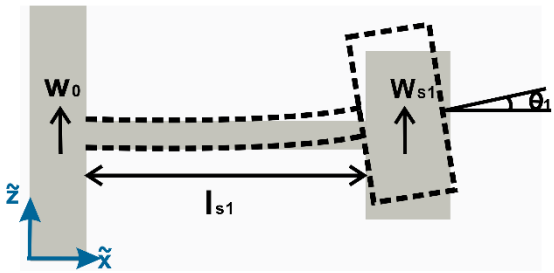

Fig. 3 Deflection of the cantilever-mass resonator

Assuming the displacement of the Π-shaped backbone is w_0 and the total displacement of the cantilever beam is $w_{s1}(\tilde{x})$, the deflection of the cantilever beam can be given as

$$\delta_1(\tilde{x}) = w_{s1}(\tilde{x}) - w_0 \tag{1}$$

Since the length of the cantilever beam is much larger than both its width and height, the cantilever beam is regarded as a Euler-Bernoulli beam. Therefore, the deflection is written as

$$\delta_1(\tilde{x}) = Q_1 e^{-ik_{s1}\tilde{x}} + Q_2 e^{-k_{s1}\tilde{x}} + Q_3 e^{ik_{s1}\tilde{x}} + Q_4 e^{k_{s1}\tilde{x}} \tag{2}$$

where $k_{s1} = (\rho A_{s1}/EI_{s1})^{1/4}\sqrt{\omega}$, ρ denotes the material density, $E = E_0(1+i\eta)$, E_0 and η are the Young's modulus and loss factor of the material respectively. $A_{s1} = h_{s1}b_{s1}$ and $I_{s1} = b_{s1}h_{s1}^3/12$ are the cross-section area and second moment of area of the cantilever beam, respectively.

At the fixed point, the deflection and slope of the beam are both zero, i.e.

$$\delta_1|_{\tilde{x}=0} = 0 \tag{3}$$

$$\delta_1'|_{\tilde{x}=0} = 0 \tag{4}$$

while at the interface of mass and cantilever beam, the shearing force of cantilever beam is subjected to

$$EI_{s1}\,\delta_1'''\Big|_{\tilde{x}=l_{s1}} - m_{r1}\,\ddot{w}_{s1}|_{\tilde{x}=l_{s1}} = 0 \tag{5}$$

where $m_{r1} = \rho h_{r1} g_{r1} b_{r1}$ represents the mass of the resonator, and E is the Young's modulus of the beam. Given the rotation angle θ_1 of the mass as shown in Fig. 3, the

bending moment of cantilever beam is subjected to

$$EI_{s1}\,\delta_1''\Big|_{\tilde{x}=l_{s1}}+J_{r1}\ddot{\theta}_1=0 \tag{6}$$

where $J_{r1}=m_{r1}\left(g_{r1}^2/3+h_{r1}^2/12\right)$ represents the moment of inertia of the mass. Since the rotation angle of the mass is small, it can be approximated to

$$\theta_1\approx\tan\theta_1\approx\delta_1'\big|_{\tilde{x}=l_{s1}} \tag{7}$$

Therefore, Eqs. (5) and (6) can be rewritten as

$$EI_{s1}\,\delta_1'''\Big|_{\tilde{x}=l_{s1}}+m_{r1}\omega^2\,w_{s1}\big|_{\tilde{x}=l_{s1}}=0 \tag{8}$$

$$EI_{s1}\,\delta_1''\Big|_{\tilde{x}=l_{s1}}-J_{r1}\omega^2\,\delta_1'\Big|_{\tilde{x}=l_{s1}}=0 \tag{9}$$

Substituting Eq. (2) into Eqs. (3)-(4) and (8)-(9), the unknow parameters Q_1, Q_2, Q_3 and Q_4 are given as

$$\begin{bmatrix}Q_1\\Q_2\\Q_3\\Q_4\end{bmatrix}=\mathbf{T}_s^{-1}\begin{bmatrix}0\\0\\-m_{r1}\omega^2w_0\\0\end{bmatrix} \tag{10}$$

where $\mathbf{T}_s$ is

$$\mathbf{T}_s=\begin{bmatrix}1 & 1 & 1 & 1\\ -\mathrm{i}k_{s1} & -k_{s1} & \mathrm{i}k_{s1} & k_{s1}\\ \left(\begin{matrix}\mathrm{i}EI_{s1}k_{s1}^3\\+m_{r1}\omega^2\end{matrix}\right)\mathrm{e}^{-\mathrm{i}k_{s1}l_{s1}} & \left(\begin{matrix}-EI_{s1}k_{s1}^3\\+m_{r1}\omega^2\end{matrix}\right)\mathrm{e}^{-k_{s1}l_{s1}} & \left(\begin{matrix}-\mathrm{i}EI_{s1}k_{s1}^3\\+m_{r1}\omega^2\end{matrix}\right)\mathrm{e}^{\mathrm{i}k_{s1}l_{s1}} & \left(\begin{matrix}EI_{s1}k_{s1}^3\\+m_{r1}\omega^2\end{matrix}\right)\mathrm{e}^{k_{s1}l_{s1}}\\ \left(\begin{matrix}-EI_{s1}k_{s1}^2\\+\mathrm{i}k_{s1}J_{r1}\omega^2\end{matrix}\right)\mathrm{e}^{-\mathrm{i}k_{s1}l_{s1}} & \left(\begin{matrix}EI_{s1}k_{s1}^2\\+J_{r1}\omega^2k_{s1}\end{matrix}\right)\mathrm{e}^{-k_{s1}l_{s1}} & \left(\begin{matrix}-EI_{s1}k_{s1}^2\\-\mathrm{i}k_{s1}J_{r1}\omega^2\end{matrix}\right)\mathrm{e}^{\mathrm{i}k_{s1}l_{s1}} & \left(\begin{matrix}EI_{s1}k_{s1}^2\\-J_{r1}\omega^2k_{s1}\end{matrix}\right)\mathrm{e}^{k_{s1}l_{s1}}\end{bmatrix} \tag{11}$$

At one end of the cantilever beam, the force exerted on the Π-shaped beam by the cantilever-mass resonator is given by

$$F_{s1}=-EI_{s1}\,\delta_1'''\Big|_{\tilde{x}=0}=-EI_{s1}k_{s1}^3\left(\mathrm{i}Q_1-Q_2-\mathrm{i}Q_3+Q_4\right)=N_{s1}w_0 \tag{12}$$

where $N_{s1}=-EI_{s1}k_{s1}^3m_{r1}\omega^2\left(-\mathrm{i}\mathbf{T}_s^{-1}(1,3)+\mathbf{T}_s^{-1}(2,3)+\mathrm{i}\mathbf{T}_s^{-1}(3,3)-\mathbf{T}_s^{-1}(4,3)\right)$.

Given the above, the interaction force between the non-symmetric resonators and the Π-shaped beam unit cell is

$$F_t=F_{s1}+F_{s2}=\left(N_{s1}+N_{s2}\right)w_0 \tag{13}$$

where F_{s2} represents the exerted force by the other resonator. F_{s2} and N_{s2} can be deduced following the same derivation procedures for F_{s1} and N_{s1}.

It is assumed that the mass of resonators is much smaller than that of Π-shaped beam, rotation of beam by the non-symmetric resonators is ignored for simplicity.

2.2 Displacement transfer matrix of the rainbow metamaterial

For a Π-shaped beam with resonators partitioned by periodical plate insertions, the schematic diagram of the nth and $(n+1)$th segments of the complex beam can be seen in Fig. 4, where $p_i L_d$ $(i=1,2,...)$ represents the locations of both resonators inside the ith segment.

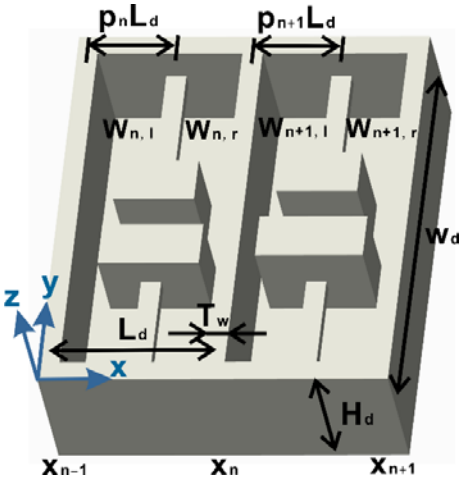

Fig. 4 Schematic diagram of nth and $(n+1)$th segments of the rainbow metamaterial

Assuming a Euler-Bernoulli beam theory, displacements of the Π-shaped beam at the left and right sides of (before and after) the local resonators inside the nth segment can be written as,

$$w_{n,l} = \alpha_{n,l} e^{-ik(x-x_{n-1})} + \beta_{n,l} e^{-k(x-x_{n-1})} + \chi_{n,l} e^{ik(x-x_{n-1})} + \varepsilon_{n,l} e^{k(x-x_{n-1})} \tag{14}$$

$$w_{n,r} = \alpha_{n,r} e^{-ik(x-(x_{n-1}+p_n L_d))} + \beta_{n,r} e^{-k(x-(x_{n-1}+p_n L_d))} + \chi_{n,r} e^{ik(x-(x_{n-1}+p_n L_d))} + \varepsilon_{n,r} e^{k(x-(x_{n-1}+p_n L_d))} \tag{15}$$

where $k=(\rho A/EI_z)^{1/4}\sqrt{\omega}$, $A=w_d b_d + 2t_d H_d$ represents the cross-section area of the Π-shaped beam. I_z is the second moment of area of the Π-shaped beam about its centroidal axis, given as

$$I_z \approx \frac{H_d^4 t_d^2 + 2t_d H_d^3 w_d b_d}{3A} \tag{16}$$

As discussed in Section 2.1, the interaction between the cantilever-mass resonators

and Π-shaped beam is expressed by a force F_t. Therefore, the continuity of displacement, slope and equilibrium of bending moment and shearing force at the fixed point of the cantilever beam should be

$$\begin{aligned} w_{n,l}\big|_{x=x_{n-1}+p_nL_d} &= w_{n,r}\big|_{x=x_{n-1}+p_nL_d} \\ w'_{n,l}\big|_{x=x_{n-1}+p_nL_d} &= w'_{n,r}\big|_{x=x_{n-1}+p_nL_d} \\ w''_{n,l}\big|_{x=x_{n-1}+p_nL_d} &= w''_{n,r}\big|_{x=x_{n-1}+p_nL_d} \\ EI_z\, w'''_{n,l}\big|_{x=x_{n-1}+p_nL_d} + F_{t,n} &= EI_z\, w'''_{n,r}\big|_{x=x_{n-1}+p_nL_d} \end{aligned} \tag{17}$$

Substituting Eqs. (13), (14) and (15) into Eq. (17), yields

$$\begin{bmatrix} \alpha_{n,r} \\ \beta_{n,r} \\ \chi_{n,r} \\ \varepsilon_{n,r} \end{bmatrix} = \mathbf{R}_c^{-1}\mathbf{R}_n\mathbf{\Lambda}_{n,l} \begin{bmatrix} \alpha_{n,l} \\ \beta_{n,l} \\ \chi_{n,l} \\ \varepsilon_{n,l} \end{bmatrix} \tag{18}$$

where the matrices $\mathbf{R}_c$, $\mathbf{R}_n$ and $\mathbf{\Lambda}_{n,l}$ are given as

$$\mathbf{R}_c = \begin{bmatrix} 1 & 1 & 1 & 1 \\ -\mathrm{i} & -1 & \mathrm{i} & 1 \\ -1 & 1 & -1 & 1 \\ \mathrm{i}EI_zk^3 & -EI_zk^3 & -\mathrm{i}EI_zk^3 & EI_zk^3 \end{bmatrix}$$

$$\mathbf{R}_n = \begin{bmatrix} 1 & 1 & 1 & 1 \\ -\mathrm{i} & -1 & \mathrm{i} & 1 \\ -1 & 1 & -1 & 1 \\ \left(\mathrm{i}EI_zk^3 + N_{s,n}\right) & \left(-EI_zk^3 + N_{s,n}\right) & \left(-\mathrm{i}EI_zk^3 + N_{s,n}\right) & \left(EI_zk^3 + N_{s,n}\right) \end{bmatrix} \tag{19}$$

$$\mathbf{\Lambda}_{n,l} = \mathrm{diag}\left(\mathrm{e}^{-\mathrm{i}kp_nL_d}, \mathrm{e}^{-kp_nL_d}, \mathrm{e}^{\mathrm{i}kp_nL_d}, \mathrm{e}^{kp_nL_d}\right)$$

Displacements of the Π-shaped beam at the left side of the local resonators inside $(n+1)$th unit cell can be written as

$$w_{n+1,l} = \alpha_{n+1,l}\mathrm{e}^{-\mathrm{i}k(x-x_n)} + \beta_{n+1,l}\mathrm{e}^{-k(x-x_n)} + \chi_{n+1,l}\mathrm{e}^{\mathrm{i}k(x-x_n)} + \varepsilon_{n+1,l}\mathrm{e}^{k(x-x_n)} \tag{20}$$

To find out the displacement transfer matrix between the nth and $(n+1)$th unit cell, the plate insertions are modeled as added masses to the Π-shaped beam. At the interface of the two segments, considering the continuity of displacement, slope and equilibrium of bending moment and shearing force, yields

$$
\begin{aligned}
w_{n,r}\big|_{x=x_n} &= w_{n+1,l}\big|_{x=x_n} \\
w'_{n,r}\big|_{x=x_n} &= w'_{n+1,l}\big|_{x=x_n} \\
EI_z w''_{n,r}\big|_{x=x_n} - J_f\omega^2 w'_{n,r}\big|_{x=x_n} &= EI_z\, w''_{n+1,l}\big|_{x=x_n} \\
EI_z\, w'''_{n,r}\big|_{x=x_n} + m_f\omega^2 w_{n,r}\big|_{x=x_n} &= EI_z\, w'''_{n+1,l}\big|_{x=x_n}
\end{aligned}
\tag{21}
$$

where $m_f = \rho t_w H_d w_d$ and $J_f = m_f\left(H_d^2/3 + t_w^2/12\right)$ are the mass and moment of inertia of the plate insertions respectively.

Substituting Eqs. (15) and (20) into Eq. (21), yields

$$
\begin{bmatrix} \alpha_{n+1,l} \\ \beta_{n+1,l} \\ \chi_{n+1,l} \\ \varepsilon_{n+1,l} \end{bmatrix} = \mathbf{R}^{-1}\mathbf{U}\mathbf{\Lambda}_{n,r} \begin{bmatrix} \alpha_{n,r} \\ \beta_{n,r} \\ \chi_{n,r} \\ \varepsilon_{n,r} \end{bmatrix} \tag{22}
$$

where

$$
\mathbf{\Lambda}_{n,r} = \mathrm{diag}\left(\mathrm{e}^{-\mathrm{i}k(1-p_n)L_d}, \mathrm{e}^{-k(1-p_n)L_d}, \mathrm{e}^{\mathrm{i}k(1-p_n)L_d}, \mathrm{e}^{k(1-p_n)L_d}\right)
$$

$$
\mathbf{R} = \begin{bmatrix} 1 & 1 & 1 & 1 \\ -\mathrm{i} & -1 & \mathrm{i} & 1 \\ -EI_z k^2 & EI_z k^2 & -EI_z k^2 & EI_z k^2 \\ \mathrm{i}EI_z k^3 & -EI_z k^3 & -\mathrm{i}EI_z k^3 & EI_z k^3 \end{bmatrix} \tag{23}
$$

$$
\mathbf{U} = \begin{bmatrix} 1 & 1 & 1 & 1 \\ -\mathrm{i} & -1 & \mathrm{i} & 1 \\ \left(-EI_z k^2 + \mathrm{i}J_f\omega^2 k\right) & \left(EI_z k^2 + J_f\omega^2 k\right) & \left(-EI_z k^2 - \mathrm{i}J_f\omega^2 k\right) & \left(EI_z k^2 - J_f\omega^2 k\right) \\ \left(\mathrm{i}EI_z k^3 + m_f\omega^2\right) & \left(-EI_z k^3 + m_f\omega^2\right) & \left(-\mathrm{i}EI_z k^3 + m_f\omega^2\right) & \left(EI_z k^3 + m_f\omega^2\right) \end{bmatrix}
$$

Thus, the displacement transfer matrix of the metamaterial is expressed by

$$
\begin{bmatrix} \alpha_{n+1,l} \\ \beta_{n+1,l} \\ \chi_{n+1,l} \\ \varepsilon_{n+1,l} \end{bmatrix} = \mathbf{T}_n \begin{bmatrix} \alpha_{n,l} \\ \beta_{n,l} \\ \chi_{n,l} \\ \varepsilon_{n,l} \end{bmatrix} = \mathbf{T}_n \mathbf{T}_{n\text{-}1} \cdots \mathbf{T}_1 \begin{bmatrix} \alpha_{1,l} \\ \beta_{1,l} \\ \chi_{1,l} \\ \varepsilon_{1,l} \end{bmatrix} \tag{24}
$$

where $\mathbf{T}_n = \mathbf{R}^{-1}\mathbf{U}\mathbf{\Lambda}_{n,r}\mathbf{R}_c^{-1}\mathbf{R}_n\mathbf{\Lambda}_{n,l}$. The transfer matrix is applicable for both periodic and rainbow metamaterial beams.

2.3 Determining the Frequency Response Function of finite rainbow metamaterial

For a rainbow metamaterial of finite length, the displacements at the two ends of the complex beam can be given as,

$$
w_{1,l}\big|_{x=0} = \alpha_{1,l} + \beta_{1,l} + \chi_{1,l} + \varepsilon_{1,l} \tag{25}
$$

$$w_{m,r}\big|_{x=L}=\alpha_{m,r}\mathrm{e}^{-\mathrm{i}k(1-p_m)L_d}+\beta_{m,r}\mathrm{e}^{-k(1-p_m)L_d}+\chi_{m,r}\mathrm{e}^{\mathrm{i}k(1-p_m)L_d}+\varepsilon_{m,r}\mathrm{e}^{k(1-p_m)L_d} \tag{26}$$

where L and $m=L/L_d$ are the length and the number of segments of the finite metamaterial respectively.

Relations between the two matrices $\left[\alpha_{1,l}\ \beta_{1,l}\ \chi_{1,l}\ \varepsilon_{1,l}\right]^{\mathrm{T}}$ and $\left[\alpha_{m,r}\ \beta_{m,r}\ \chi_{m,r}\ \varepsilon_{m,r}\right]^{\mathrm{T}}$ are deduced by combing Eqs. (18) with (24),

$$\begin{bmatrix}\alpha_{m,r}\\ \beta_{m,r}\\ \chi_{m,r}\\ \varepsilon_{m,r}\end{bmatrix}=\mathbf{\Pi}\begin{bmatrix}\alpha_{1,l}\\ \beta_{1,l}\\ \chi_{1,l}\\ \varepsilon_{1,l}\end{bmatrix} \tag{27}$$

where $\mathbf{\Pi}=\mathbf{R}_c^{-1}\mathbf{R}_m\mathbf{\Lambda}_{m,l}\mathbf{T}_{m-1}\mathbf{T}_{m-2}\cdots\mathbf{T}_1$.

Assuming the finite metamaterial is of free-free boundary and subjected to an excitation F at one end, given the equilibrium conditions, governing equations at the two ends are,

$$F+m_f\omega^2\,w_{1,l}\big|_{x=x_0}=EI_z\,w_{1,l}'''\big|_{x=x_0} \tag{28}$$

$$-J_f\omega^2\,w_{1,l}'\big|_{x=x_0}=EI_z\,w_{1,l}''\big|_{x=x_0} \tag{29}$$

$$EI_z\,w_{m,r}'''\big|_{x=L}+m_f\omega^2\,w_{m,r}\big|_{x=L}=0 \tag{30}$$

$$EI_z\,w_{m,r}''\big|_{x=L}-J_f\omega^2\,w_{m,r}'\big|_{x=L}=0 \tag{31}$$

According to Eqs. (28)-(31), one obtains

$$\mathbf{\Psi}\begin{bmatrix}\alpha_{1,l}\\ \beta_{1,l}\\ \chi_{1,l}\\ \delta_{1,l}\end{bmatrix}=\begin{bmatrix}0\\ F\\ 0\\ 0\end{bmatrix} \tag{32}$$

where $\mathbf{\Psi}=\left[\mathbf{\Psi}_1\ \mathbf{\Psi}_2\right]^{\mathrm{T}}$, $\mathbf{\Psi}_1$ and $\mathbf{\Psi}_2$ are given as

$$\mathbf{\Psi}_1=\begin{bmatrix}\left(-EI_zk^2-\mathrm{i}kJ_f\omega^2\right) & \left(EI_zk^2-kJ_f\omega^2\right) & \left(-EI_zk^2+\mathrm{i}kJ_f\omega^2\right) & \left(EI_zk^2+kJ_f\omega^2\right)\\ \left(EI_z\mathrm{i}k^3-m_f\omega^2\right) & \left(-EI_zk^3-m_f\omega^2\right) & \left(-EI_z\mathrm{i}k^3-m_f\omega^2\right) & \left(EI_zk^3-m_f\omega^2\right)\end{bmatrix} \tag{33}$$

$$\mathbf{\Psi}_2=\begin{bmatrix}\left(-EI_zk^2+\mathrm{i}J_f\omega^2k\right) & \left(EI_zk^2+J_f\omega^2k\right) & \left(-EI_zk^2-\mathrm{i}J_f\omega^2k\right) & \left(EI_zk^2-J_f\omega^2k\right)\\ \left(EI_z\mathrm{i}k^3+m_f\omega^2\right) & \left(-EI_zk^3+m_f\omega^2\right) & \left(-EI_z\mathrm{i}k^3+m_f\omega^2\right) & \left(EI_zk^3+m_f\omega^2\right)\end{bmatrix}\mathbf{\Lambda}_{m,r}\mathbf{\Pi} \tag{34}$$

Based on Eq. (32), the unknown parameters are derived as

$$\begin{bmatrix} \alpha_{1,l} \\ \beta_{1,l} \\ \chi_{1,l} \\ \varepsilon_{1,l} \end{bmatrix} = \boldsymbol{\Psi}^{-1} \begin{bmatrix} 0 \\ F \\ 0 \\ 0 \end{bmatrix}$$
$$\begin{bmatrix} \alpha_{m,r} \\ \beta_{m,r} \\ \chi_{m,r} \\ \varepsilon_{m,r} \end{bmatrix} = \boldsymbol{\Pi}\boldsymbol{\Psi}^{-1} \begin{bmatrix} 0 \\ F \\ 0 \\ 0 \end{bmatrix} \tag{35}$$

Substituting Eq. (35) into Eqs. (25) and (26), the displacement of the metamaterial with excitation F at one end can be obtained. Furthermore, the receptance function of the rainbow metamaterial is derived by,

$$R_{ec} = 20\log_{10}\left|\frac{w_{m,r}\big|_{x=L}}{F}\right| \tag{36}$$

In addition, according to the Bloch theorem [29], the wave number q of the periodic metamaterial can be defined from transfer matrix

$$\begin{bmatrix} \alpha_{n+1,l} \\ \beta_{n+1,l} \\ \chi_{n+1,l} \\ \varepsilon_{n+1,l} \end{bmatrix} = \mathbf{T}_n \begin{bmatrix} \alpha_{n,l} \\ \beta_{n,l} \\ \chi_{n,l} \\ \varepsilon_{n,l} \end{bmatrix} = \mathrm{e}^{\mathrm{i}qL_d} \begin{bmatrix} \alpha_{n,l} \\ \beta_{n,l} \\ \chi_{n,l} \\ \varepsilon_{n,l} \end{bmatrix} \tag{37}$$

that is

$$\left|\mathbf{T}_n - \mathrm{e}^{\mathrm{i}qL}\mathbf{I}\right| = 0 \tag{38}$$

By analogy of the wavenumber of periodic metamaterials, an equivalent wavenumber q^* is defined for the finite length rainbow metamaterial with spatially varying resonators, as

$$\left|\boldsymbol{\Xi} - \mathrm{e}^{\mathrm{i}q^*L}\mathbf{I}\right| = 0 \tag{39}$$

where $\boldsymbol{\Xi}=\mathbf{T}_m\mathbf{T}_{m-1}...\mathbf{T}_1$. The equivalent wavenumber q^* can be also interpreted as the wavenumber when the finite rainbow metamaterial is a periodic unit of an infinite complex beam. It is used as a tool to understand the wave-like behavior of non-periodic structures.

3. Prototype manufacturing and experimental validation

To verify the proposed mathematical model, a receptance measuring experiment was performed with the rainbow metamaterials produced by additive manufacturing (AM) method. AM is becoming a common method for manufacturing of

elastic/acoustic metamaterials with complex geometries [48-51]. AM technologies create structures in a layer-by-layer process, either through material deposition or by selective solidification of a feedstock. AM technologies can fabricate complex structures that are impossible or not feasible to fabricate by traditional manufacturing methods, hence attract much attention from researchers from many fields. Specifically, the emergence of a variety of AM technologies, such as powder bed fusion, material jetting, stereolithography and binder jetting, allows for the fabrication of structures with different materials, dimensions and accuracies.

Two metamaterial samples were fabricated by the powder bed fusion process depicted in Fig. 5 using an EOS Formiga P100 machine with Nylon-12 employed to fill the powder bed.

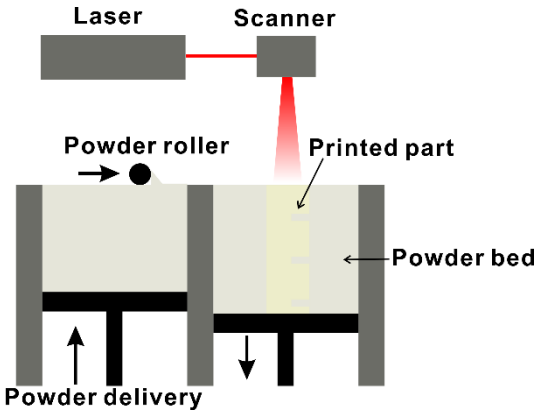

Fig. 5 Schematic illustration of the powder bed fusion process

One sample of the printed metamaterials is shown in Fig. 6. The tested metamaterial is stuck firmly to the shaker at one end with the Ethyl 2-cyanoacrylate superglue. The printed structures have nominal density of 930 kg/m^3, a Young's Modulus of 1.8 GPa, a Poisson's ratio of 0.3, and a loss factor of 0.03. The density of the samples was estimated by the ratio of mass and volume, and Young's Modulus was obtained by testing structures printed by the same material and AM method with the universal testing machine. Geometrical parameters of the two printed metamaterials are listed in Table 1.

Table 1 Geometrical parameters of tested rainbow metamaterials.

Π-shaped beam with plate insertions	
Height	$H_d = 10$ mm
Width	$w_d = 51$ mm
Side wall thickness	$t_d = 2$ mm
Backplate thickness	$b_d = 5$ mm
Plate insertion thickness	$t_w = 2$ mm
Distance between plate insertions	$L_d = 15$ mm

Number of segments	$m = 17$
Total length of metamaterial beams	$L = 0.257$ m
Cantilever beam	
Sample 1#	
Height	$h_{s1} = h_{s2} = 1.4$ mm
Width	$b_{s1} = b_{s2} = 1.9$ mm
Length	$l_{s1} = l_{s2} = 21.2$ mm
Sample 2#	
Height	$h_{s1} = 1.4$ mm, $h_{s2} = 2.3$ mm
Width	$b_{s1} = 1.9$ mm, $b_{s2} = 2.3$ mm
Length	$l_{s1} = l_{s2} = 21.2$ mm

The measurement system consists of a mechanical shaker, a vibrometer, sensors and auxiliary components as shown in Fig. 7. A junction box follows the command by computer and generates the vibration signal, which controls the exciting force of the shaker after amplification. The tested metamaterials are excited by the mechanical shaker at one end. The actual exciting force is measured by a force sensor attached to the metamaterial, and the displacement of the metamaterial at the other end measured by a laser vibrometer. A cooling system is connected to the shaker. In the experiment we used the Modal Shop 2060E shaker, PCB 288D01 impedance head that contains a force sensor, Polytec PDV-100 portable digital laser vibrometer and Polytec VIB-E-400 junction box. A chirp signal was used as input signal of the shaker.

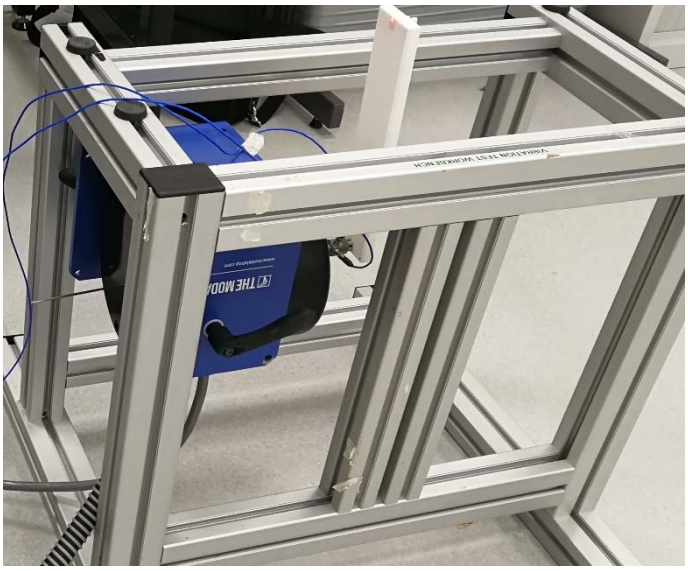

Fig.6 Experimental setup of a rainbow metamaterial sample.

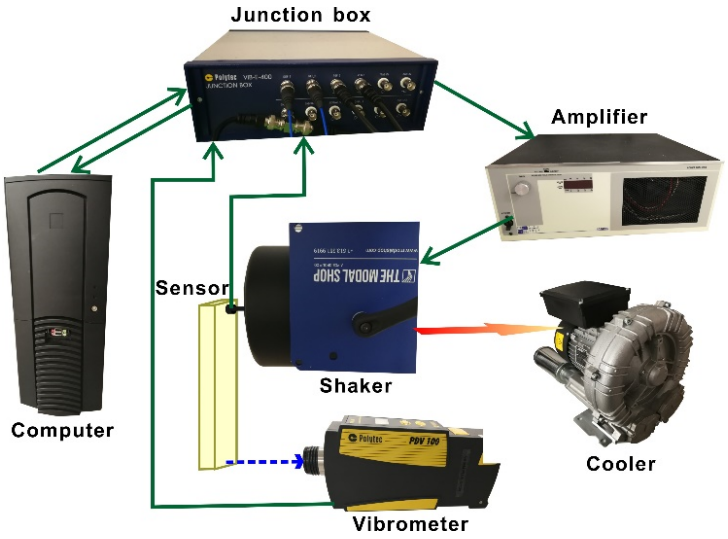

Fig.7 Experimental setup for receptance tests of the rainbow metamaterials.

The mathematical results are shown with the experimental measurements in Figs. 8(a) and (b). Ratios of resonator mass to a reference mass m_c of the two metamaterials are also plotted in Figs. 8(a) and (b). The reference mass m_c is derived as

$$m_c = \frac{M_t}{m} \tag{40}$$

where M_t are the total mass of the Π-shaped beam and plate insertions.

It can be seen from Figs. 8(a) and (b) that the mathematical results are in good agreement with the experimental ones. For sample $1^{\#}$ with symmetric resonators, one bandgap can be seen in both the mathematical and experimental curves as shown in Fig. 8(a). As to sample $2^{\#}$ with non-symmetric resonators, the two bandgap regions being obvious exist in both experimental and mathematical curves as shown in Fig. 8(b). The discrepancies between the experimental and mathematical results lie in the bandgap frequencies, which might be attributed to the dimension and physical parameter variability of the tested samples, as well as to the uncertainty introduced by the manufacturing and experimental conditions. Although the manufacturing variability can play an important role on the metamaterial performance [52], this issue will be addressed in further work. In addition, the discrepancies might be attributed to modelling assumptions which consider only idealized flexural deformation of the Π-shaped beam for simplicity. Other minor deformations, such as local deformation in the cross section introduced by forces of resonators at two side walls, might occur in the experiment and affect the stiffness of the structure, hence result in differences between predicted and measured results. Especially, the local deformation by non-symmetric resonators could be larger than that by symmetric resonator, discrepancies of

metamaterial beam with non-symmetric resonators are hence enhanced compared with that of metamaterial beam with symmetric resonator as shown in Figs. 8(a) and (b).

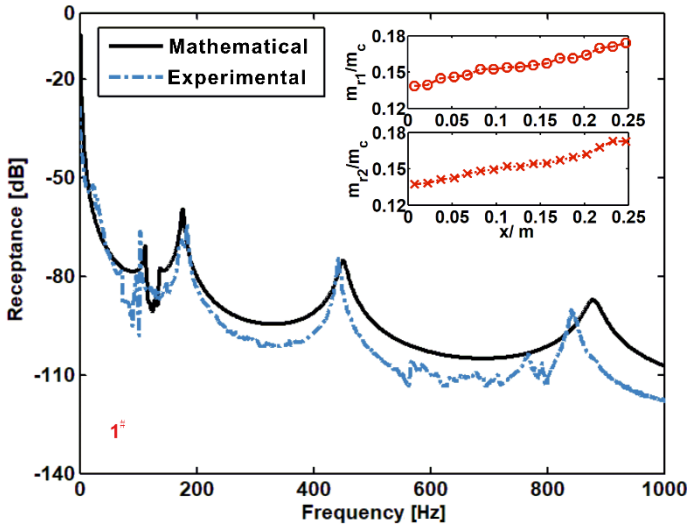

(a)

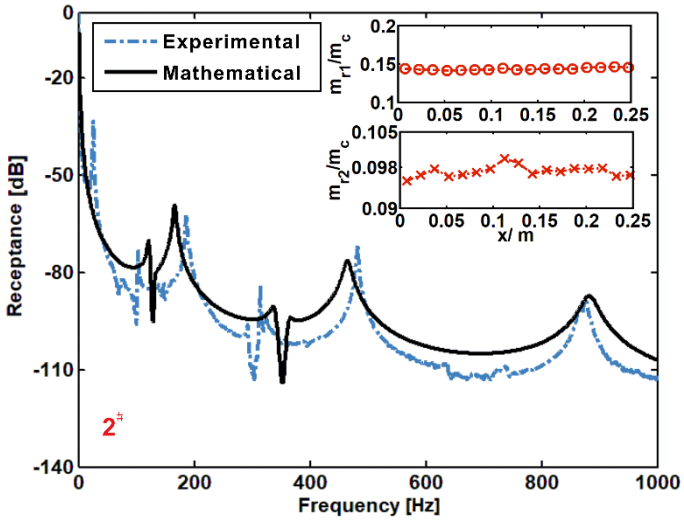

(b)

Fig.8 Amplitude of transfer receptance comparison between mathematical (——) and experimental (- - -) results (a) Sample 1#, (b) Sample 2#. The mass distributions are also plotted in the subfigures.

4. Numerical study

In this section, a numerical study is conducted to explore the influence of resonator distributions on the FRF performance of the metamaterial. On the basis of the abovementioned mathematical model, dispersion curves and receptance functions of rainbow metamaterials are compared with that of metamaterials with periodic resonators. Besides, differences of dispersion curves and receptance due to symmetric and non-symmetric resonators are also discussed in this section. The calculated samples have a density of 1010 kg/m^3, a Young's Modulus of 1.2 GPa, a Poisson's ratio of 0.3,

and a loss factor of 0.02. Geometrical parameters of the calculated structures are listed in Table 2.

Table 2 Geometrical parameters of calculated rainbow metamaterials

Π-shaped beam	
Height	$H_d = 10$ mm
Width	$w_d = 49$ mm
Side wall thickness	$t_d = 2$ mm
Backplate thickness	$b_d = 5$ mm
Plate insertion thickness	$t_w = 2$ mm
Distance between plate insertions	$L_d = 15$ mm
Number of segments	$m = 30$
Total length of metamaterial	$L = 0.45$ m
Cantilever beam	
Height	$h_{s1} = h_{s2} = 1.5$ mm
Width	$b_{s1} = b_{s2} = 2$ mm
Length	$l_{s1} = l_{s2} = 21$ mm

4.1 Metamaterial beams with symmetric periodic cantilever-mass resonators

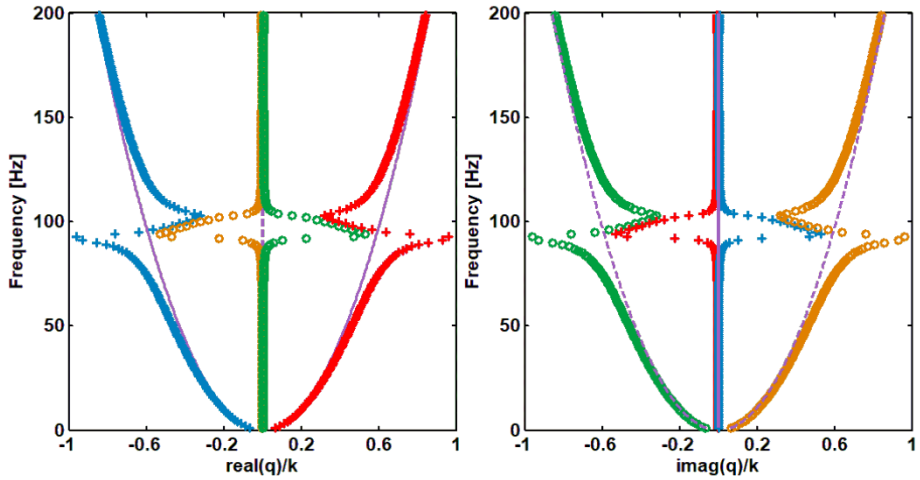

Fig. 9 Wavenumbers of a metamaterial beam with periodic cantilever-mass resonators. The cross lines (+++) and dot lines (ooo) represent waves in the complex beam with resonators, and solid and dashed lines (---) represent the waves in beam without resonators .

The obtained wavenumbers of the metamaterial beam with symmetric periodic cantilever-mass resonators are shown in Fig. 9. r represents the mass ratio of all

resonators to the metamaterial beam. The ratio r of the calculated beam shown in Fig. 9 is 20%. The wavenumbers of the bare beam without resonators are also plotted for comparison.

It can be seen from Fig. 9 that two kinds of waves, propagating and evanescent waves, exist inside the beams. For a lossless beam, propagating waves refer to the waves whose wavenumbers have purely real components, such that they are oscillatory and propagate inside the structure. In addition, evanescent waves refer to exponentially decaying waves as their imaginary parts of wavenumbers have relatively big absolute values. The two propagating waves and evanescent waves are easily distinguished in the considered frequency regime for the bare beam without resonators. With regard to the metamaterial beam, wavenumbers of all the four waves have both imaginary and real components inside the bandgap regime, which means purely propagating waves do not exist. The large contribution of the imaginary part leads to a rapidly decay and ensures no wave propagation as expected.

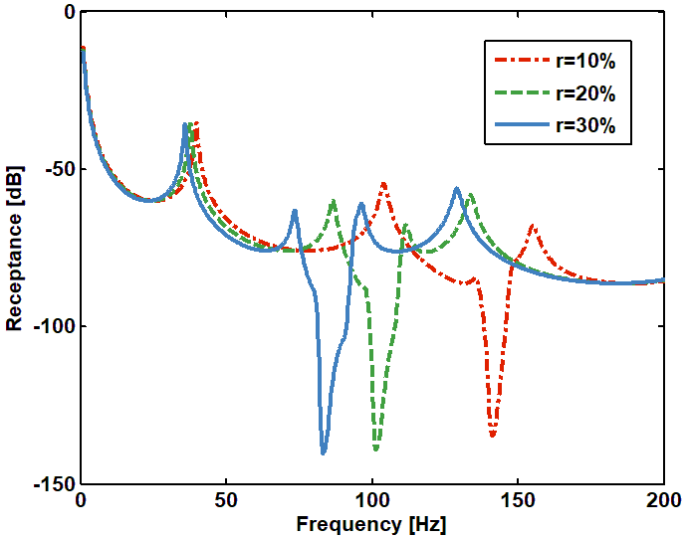

Fig. 10 Amplitude of the transfer receptance of the metamaterial beams with symmetric periodic cantilever-mass resonators of different mass.

Next, we consider the transfer receptance of finite metamaterial beams with symmetric periodic resonators (see Fig. 10). The ratios r are 10%, 20% and 30% respectively. It can be seen from Fig. 10 that a single sharp dip appears in each of the receptance curves. As discussed in the last paragraph, the periodic resonators can suppress vibration by inducing strong attenuation. Hence, a bandgap in which no waves are transmitted will be generated. Besides, it also can be seen that the bandgap shifts to lower frequencies for increasing mass of the resonators. Likewise, the cantilever-mas resonance frequency decreases when the mass increases, the bandgap frequencies decrease accordingly. It is impressive to observe that additional resonating mass does not have a drastic impact on the depth of the bandgap.

4.2 Metamaterial beams with symmetric rainbow-shaped cantilever-mass resonators

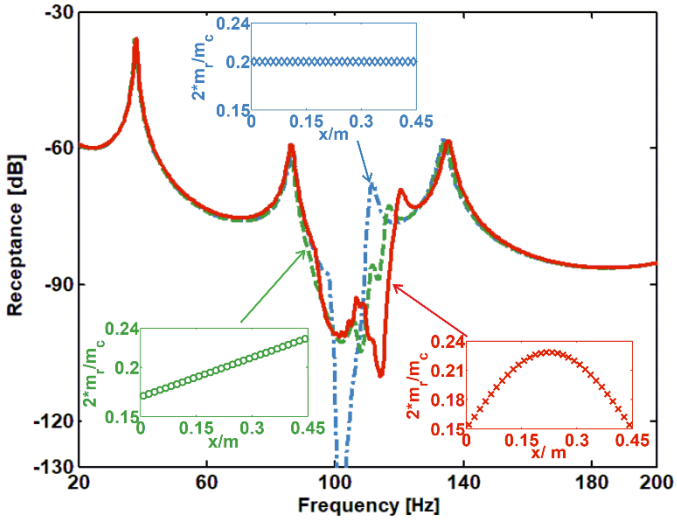

Fig. 11 Amplitude of the transfer receptance function of the metamaterial beam with symmetric uniform (- · ·), linearly varying (- - -) and sinusoidally varying (——) cantilever-mass resonators ($r = 20\%$). The mass distributions of the structures are plotted in each corresponding subfigure.

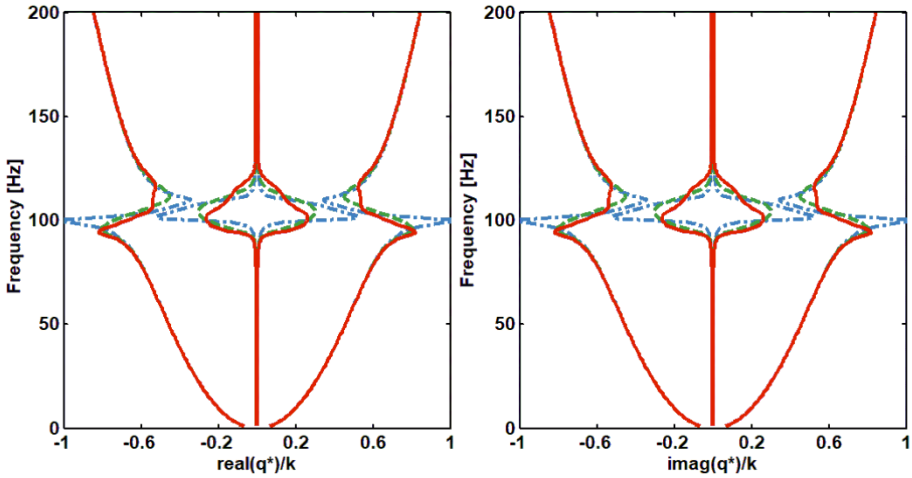

Fig. 12 Equivalent wavenumber of the metamaterial beam with symmetric uniform (- · ·), linearly varying (- -) and sinusoidally varying (——) cantilever-mass resonators ($r = 20\%$).

In order to reveal the influence of the rainbow-shaped resonators and explore helpful design routes for the rainbow metamaterials, we consider beams with non-periodically distributed resonators, i.e. linearly and sinusoidally varying resonators. More complex distributions can be piled up on the basis of simple ones. The obtained transfer receptance and wavenumbers of the metamaterial beams with symmetric periodic and spatially varying resonators are compared in Figs. 11 and 12, respectively. The total mass ratio of the resonators is identical for the three cases, $r = 20\%$. The ratio of each resonating mass to a reference mass m_c is also plotted in Fig. 11.

It can be seen from Fig. 11 that when compared to a metamaterial beam with periodic resonators, the rainbow-shaped resonators create broader bandgap regions. Since the rainbow-shaped resonators can introduce inertia forces inside a broader frequency range, the bandwidth is hence enlarged. This can also be explained from results shown in Fig. 12. For the linearly and sinusoidally varying profiles, the imaginary part of the wavenumber gets increasingly broader while simultaneously getting smaller. This widening and reduction of the imaginary part of the wavenumber causes an increased attenuation bandwidth with smaller attenuation amplitude.

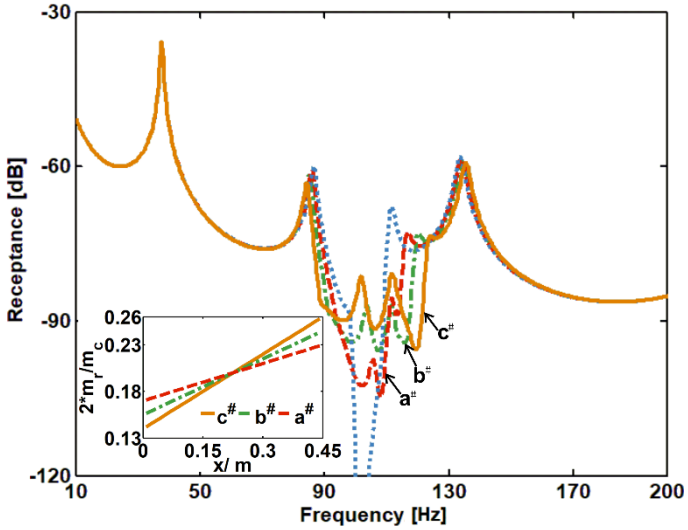

(a)

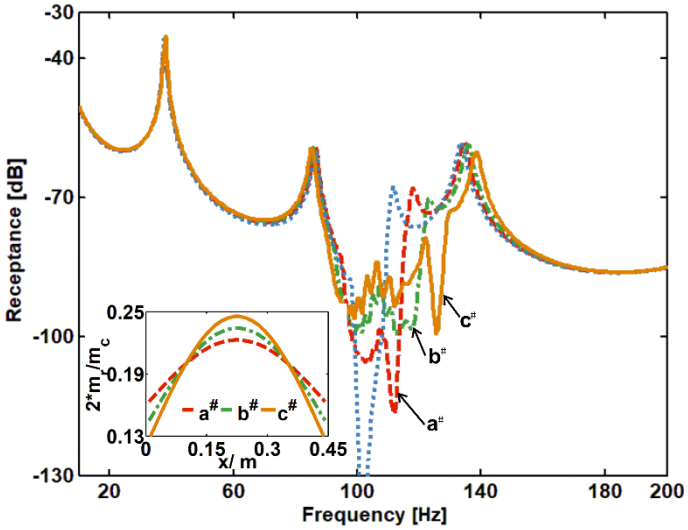

(b)

Fig. 13 Amplitude of the transfer receptance function of metamaterials with different linearly (a) and sinusoidally (b) varying resonators ($r = 20\%$). The receptance functions of metamaterials with periodic resonators are also shown (⋯⋯) for comparison. The mass distributions of these metamaterial are shown in each corresponding subfigure.

Moreover, we compare the amplitude of receptance of metamaterials with different degrees of linearly and sinusoidally distributed resonators in Figs. 13(a) and (b). The total mass of the resonators is the same for all of the cases, with a ratio $r = 20\%$. It can be seen from Fig. 13(a) that, the bandgap increases with increasing slope of the linear mass line, while the receptance reduction inside the bandgap on the contrary decreases. That is, the bandgap by local resonators could be broadened when their mass changes dramatically, which simultaneously sacrifices the attenuation amplitude inside the bandgap. The same changing pattern can be seen for metamaterials with sinusoidal resonators in Fig. 13(b). The bandgap is enlarged by increasing amplitude of the sinusoidal mass line, while the receptance reduction falls conversely. One should consider both the bandwidth and receptance of reduction when designing the rainbow metamaterials. It should also be noted that for increasingly steeper variations of the masses of the resonators, there is band gap annihilation related to the level of disorder degree. It has been shown that this is caused by internal wave trapping phenomena [52] due to the existing critical sections, i.e. local changes from propagating to non-propagating waves [53].

4.3 Metamaterial beams with non-symmetry cantilever-mass resonators

The aforementioned metamaterial beams have symmetric resonators. Even though the width of bandgaps can be enlarged by rainbow-shaped resonators, only one bandgap can be seen within the considered frequency spectrum. In order to achieve multi-frequency range vibration attenuation, beams having non-symmetric resonators are discussed in this section.

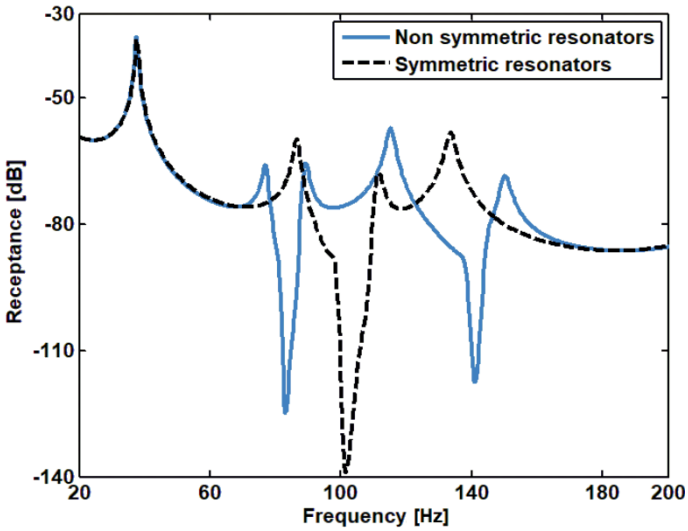

Fig. 14 Amplitude of receptance of the metamaterial beams with symmetric (---) and non-symmetric (——) periodic cantilever-mass resonators

Figure 14 shows the receptance of metamaterial beams with symmetric and non-symmetric cantilever-mass resonators. The resonators of the two metamaterial beams

in different segments are assumed to be identical, i.e. a periodic profile. The mass of symmetric resonators is $0.2M_t/2m$, while the masses of non-symmetric resonators for both sides are $0.3M_t/2m$ and $0.1M_t/2m$. The wavenumbers of the metamaterial beam with non-symmetric wavenumber are plotted in Fig. 15. It can be seen from Figs. 14 and 15 that the metamaterial beams with non-symmetric cantilever-mass resonators presents two bandgaps, at frequency ranges 79-85 Hz and 127~143 Hz. Moreover, it can be seen from Fig. 14 that the bandgap width and the attenuation of the beam with non-symmetric periodic resonators are both reduced when compared to that of beams with symmetric periodic resonators. Since the inertia forces decrease with decreasing resonator mass, the attenuation that is introduced by the non-symmetric resonators is hence weakened.

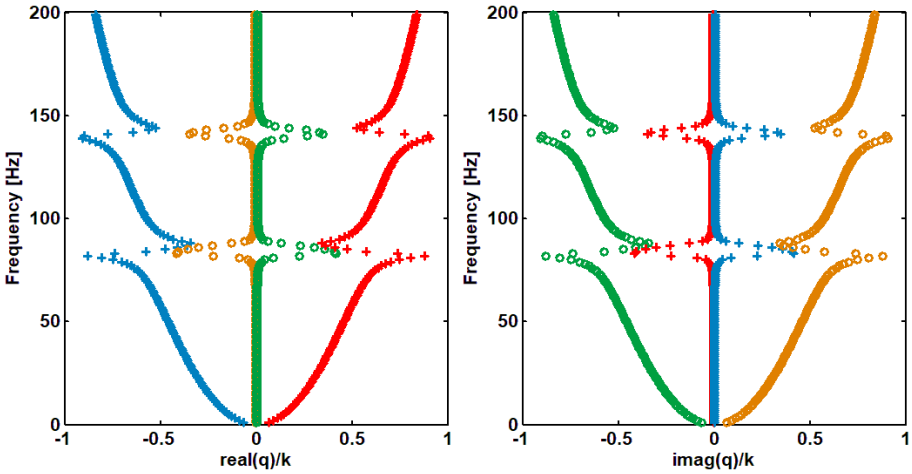

Fig. 15 Wavenumber of metamaterial beams with non-symmetric periodic cantilever-mass resonators. The cross lines (+++) and dot lines $(\circ\circ\circ)$ represent propagating waves and evanescent waves in the complex beam with resonators respectively.

The displacement of the Π-shaped beam and of both resonators along the beam are plotted in Figs. 16(a), (b) and (c). It can be seen from Figs. 16(a) and (b) that the displacements of resonators with the mass of $0.1M_t/2m$ are almost the same as that of the Π-shaped beam within the first bandgap (79-85 Hz), which means that inertia forces that attenuate the Π-shaped beam vibration is introduced by the resonators with the mass of $0.3M_t/2m$. On the contrary, the resonators with the mass $m_r = 0.3M_t/2m$ have no effect on the vibration of the Π-shaped beam within the second bandgap (127~143 Hz), the attenuation is provided by the resonators with the

mass $0.1M_t / 2m$ as shown in Figs. 16(a) and (c).

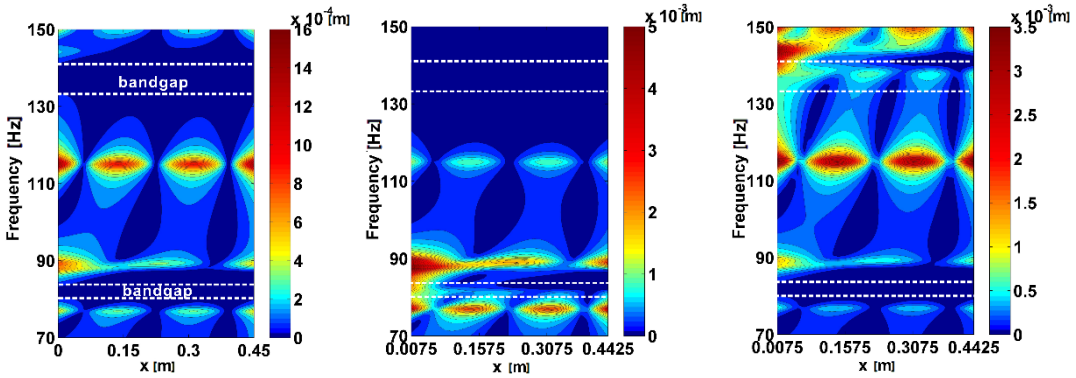

Fig. 16 Displacement amplitude of the Π-shaped beam (a), and the displacement amplitude of the resonators of mass $0.3M_t / 2m$ (b) and resonators of mass $0.1M_t / 2m$ (c) due to a point harmonic excitation at $x = 0$.

For the purpose of enlarging the bandwidth, non-symmetric rainbow shaped resonators can be further introduced as discussed in the last subsection. Figures 17 and 18 show the amplitude of receptance and equivalent wavenumber of the metamaterial beams with non-symmetric sinusoidally varying and periodic cantilever-mass resonators. It can be seen that the bandwidth is enlarged by the sinusoidally varying resonators. Therefore, broadband multi-frequency range attenuation can be achieved by beams with non-symmetric rainbow-shaped cantilever-mass resonators.

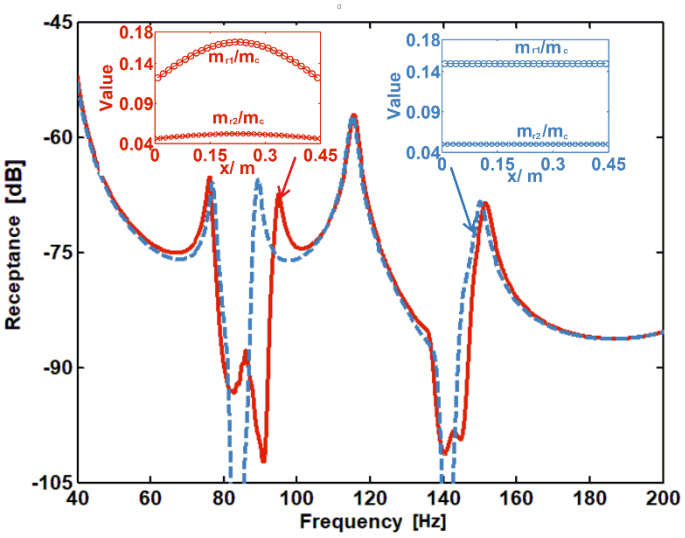

Fig. 17 Amplitude of the transfer receptance functions of the metamaterial beams with non-symmetric sinusoidally varying (——) and uniform (- - -) cantilever-mass resonators. The resonators mass distributions of the two structures are shown in each corresponding subfigure

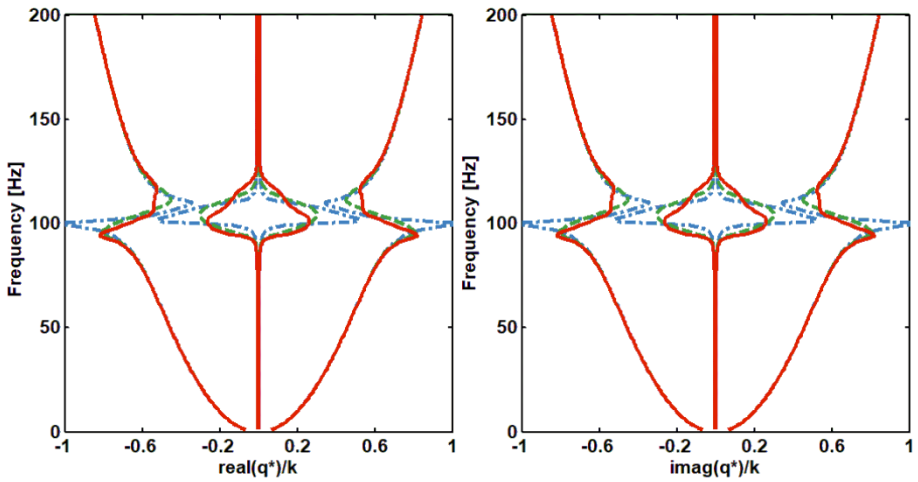

Fig. 18 Equivalent wavenumbers of metamaterial beams with non-symmetric sinusoidally varying (——) and uniform (- - -) cantilever-mass resonators.

5. Conclusions

A design of rainbow metamaterials with multi-frequency broad bandgaps was proposed in the present paper. The metamaterials were constituted of Π-shaped beams as a backbone structure with non-symmetric rainbow shaped cantilever-mass resonators partitioned by plate insertions. A mathematical model was developed to estimate the FRFs of the proposed metamaterials. The interaction forces between the Π-shaped beam and resonators were represented by calculating the displacements of the cantilever-mass structures and the plate insertions were modeled as added mass to the Π-shaped beam. Once the displacement transfer matrix between different segments of the metamaterials was obtained, the FRFs of the metamaterials could be solved out. The mathematical model was validated by experimental results. Two metamaterial structures were fabricated by AM methods and then tested with a receptance measuring system. After that, a numerical study was employed to explore the influence of the rainbow-shaped resonators on the dispersion curves and receptance of the metamaterials. Metamaterials with spatially varying resonators were proved to have broader bandgaps than that with periodic resonators, and their bandgaps can be enlarged when the resonators change dramatically. However, the broadened bandgaps result in reduced attenuation. Furthermore, metamaterials with non-symmetric resonators were found to have two bandgaps introduced by each set of resonators. Hence, multi-frequency broad bandgaps could be achieved by metamaterials with non-symmetric properly designed rainbow-shaped resonators.

Results of the present study can serve as a benchmark and be instructive for researchers in related areas to develop metamaterials with enhanced dynamic properties. The rainbow metamaterial beams with multi-frequency bandgaps could be introduced in many industrial structures as vibration attenuation and noise control systems.

Especially, the Π-shaped beam partitioned by plate insertions can be easily extended to honeycomb composites which have been widely found application in engineering fields. The proposed metamaterial beams lay the foundation stone of the future rainbow sandwich structures with enhanced vibroacoustic dissipation properties. Finally, the proposed analytical model provides an efficient tool for optimization work for the rainbow metamaterials due to its low computation cost when compared to standard FE methods. This is going to be explored in further work.

Acknowledgements

We would like to acknowledge the support acquired by the H2020 DiaMoND project (Grant Agreement ID:785859), Royal Society Grant: PURSUIT, the Brazilian National Council of Research CNPq (Grant Agreement ID: 420304/2018-5) and the Brazilian Federal District Research Foundation (Grant Agreement ID: 0193.001507/2017).

References

[1] J.B. Pendry, Negative Refraction Makes a Perfect Lens, *Phys. Rev. Lett.* 85 (2000) 3966-3969, https://journals.aps.org/prl/abstract/10.1103/PhysRevLett.85.3966

[2] J.B. Pendry, Negative refraction, *Contemp. Phys.* 45 (2004) 191-202, https://www.tandfonline.com/doi/abs/10.1080/00107510410001667434.

[3] R.A. Shelby, D.R. Smith, S. Schultz, Experimental verification of a negative index of refraction, *Science*. 292 (2001) 77-79. https://science.sciencemag.org/content/292/5514/77.abstract.

[4] T. Tanaka, A. Ishikawa, S. Kawata, Unattenuated light transmission through the interface between two materials with different indices of refraction using magnetic metamaterials, *Phys. Rev. B.* 73 (2006) 125423. https://journals.aps.org/prb/abstract/10.1103/PhysRevB.73.125423.

[5] A. Wang, A. Tuniz, P.G. Hunt, E.M. Pogson, R.A. Lewis, A. Bendavid, S.C. Fleming, B.T. Kuhlmey, M.C. Large, Fiber metamaterials with negative magnetic permeability in the terahertz, *Opt. Mater. Express.* 1 (2011) 115-120, https://www.osapublishing.org/ome/abstract.cfm?uri=ome-1-1-115.

[6] Z. Yang, H. Dai, N. Chan, G. Ma, P. Sheng, Acoustic metamaterial panels for sound attenuation in the 50–1000 Hz regime, *Appl. Phys. Lett.* 96 (2010) 041906. https://aip.scitation.org/doi/10.1063/1.3299007.

[7] T. Yamamoto, Acoustic metamaterial plate embedded with Helmholtz resonators for extraordinary sound transmission loss, *J. Appl. Phys.* 123 (2018) 215110. https://aip.scitation.org/doi/10.1063/1.5025570.

[8] H. Peng, P.F. Pai, Acoustic metamaterial plates for elastic wave absorption and structural vibration suppression, *Int. J. Mech. Sci.* 89 (2014) 350-361. https://www.sciencedirect.com/science/article/pii/S002074031400321X.

[9] X. Yong, W. Jihong, H. Lingzhi, W. Xisen, Analysis and experimental realization of locally resonant phononic plates carrying a periodic array of beam-like resonators, *J. Phys. D Appl. Phys.* 47 (2014) 045307. https://iopscience.iop.org/article/10.1088/00223727/47/4/045307.

[10] R. Zhu, X. Liu, G. Hu, C. Sun, G. Huang, A chiral elastic metamaterial beam for broadband vibration suppression, *J. Sound. Vib.* 333 (2014) 2759-2773. https://www.sciencedirect.com/science/article/pii/S0022460X14000315.

[11] S.A. Cummer, D. Schurig, One path to acoustic cloaking, *New. J. Phys.* 9 (2007) 45. https://iopscience.iop.org/article/10.1088/1367-2630/9/3/045/meta.

[12] L.-W. Cai, J. Sánchez-Dehesa, Analysis of Cummer–Schurig acoustic cloaking, *New. J. Phys.* 9 (2007) 450. https://iopscience.iop.org/article/10.1088/13672630/9/12/450/meta

[13] H. Chen, C. Chan, Acoustic cloaking in three dimensions using acoustic metamaterials, *Appl. Phys. Lett.* 91 (2007) 183518. https://aip.scitation.org/doi/10.1063/1.2803315

[14] N. Aravantinos-Zafiris, M. Sigalas, Large scale phononic metamaterials for seismic isolation, *J. Appl. Phys.* 118 (2015) 064901. https://aip.scitation.org/doi/10.1063/1.4928405

[15] Q. Du, Y. Zeng, G. Huang, H. Yang, Elastic metamaterial-based seismic shield for both Lamb and surface waves, *AIP. Adv.* 7 (2017) 075015. https://aip.scitation.org/doi/10.1063/1.4996716

[16] S.-C.S. Lin, T.J. Huang, J.-H. Sun, T.-T. Wu, Gradient-index phononic crystals, *Phys. Rev. B.* 79 (2009) 094302. https://journals.aps.org/prb/abstract/10.1103/PhysRevB.79.094302

[17] L. Morini, Y. Eyzat, M. Gei, Negative refraction in quasicrystalline multilayered metamaterials, *J. Mech. Phys. Solids.* 124 (2019) 282-298. https://www.sciencedirect.com/science/article/pii/S0022509618306410

[18] N. Jiménez, V. Romero-García, V. Pagneux, J.-P. Groby, Rainbow-trapping absorbers: Broadband, perfect and asymmetric sound absorption by subwavelength panels for transmission problems, *Sci. Rep.* 7 (2017) 13595. https://www.nature.com/articles/s41598-017-13706-4

[19] J. Zhu, Y. Chen, X. Zhu, F.J. Garcia-Vidal, X. Yin, W. Zhang, X. Zhang, Acoustic rainbow trapping, *Sci. Rep.* 3 (2013) 1728. https://www.nature.com/articles/srep01728

[20] H. Ji, J. Luo, J. Qiu, L. Cheng, Investigations on flexural wave propagation and attenuation in a modified one-dimensional acoustic black hole using a laser excitation technique, *Mech. Syst. Signal. Pr.* 104 (2018) 19-35. https://www.sciencedirect.com/science/article/pii/S0888327017305691

[21] N. Gao, Z. Wei, H. Hou, A. O. Krushynska, Design and experimental investigation of V-folded beams with acoustic black hole indentations, *J. Acoust. Soc. Am.* 145 (2019) 79-83. https://asa.scitation.org/doi/10.1121/1.5088027

[22] Z. Yang, J. Mei, M. Yang, N. Chan, P. Sheng, Membrane-type acoustic metamaterial with negative dynamic mass, *Phys. Rev. Lett.* 101 (2008) 204301. https://journals.aps.org/prl/abstract/10.1103/PhysRevLett.101.204301

[23] Z. Liu, C.T. Chan, P. Sheng, Analytic model of phononic crystals with local resonances, *Phys. Rev. B.* 71 (2005) 014103. https://journals.aps.org/prb/abstract/10.1103/PhysRevB.71.014103

[24] H.H. Huang, C.T. Sun, G.L. Huang, On the negative effective mass density in acoustic metamaterials, *Int. Journal. Eng. Sci.* 47 (2009) 610-617. https://www.sciencedirect.com/science/article/pii/S0020722508002279

[25] N. Fang, D. Xi, J. Xu, M. Ambati, W. Srituravanich, C. Sun, X. Zhang, Ultrasonic metamaterials with negative modulus, *Nat. Mater.* 5 (2006) 452. https://www.nature.com/articles/nmat1644

[26] Y. Wu, Y. Lai, Z.-Q. Zhang, Elastic Metamaterials with Simultaneously Negative Effective Shear Modulus and Mass Density, *Phys. Rev. Lett.* 107 (2011) 105506. https://journals.aps.org/prl/abstract/10.1103/PhysRevLett.107.105506

[27] S.H. Lee, C.M. Park, Y.M. Seo, Z.G. Wang, C.K. Kim, Composite acoustic medium with simultaneously negative density and modulus, *Phys. Rev. Lett.* 104 (2010) 054301. https://journals.aps.org/prl/abstract/10.1103/PhysRevLett.104.054301

[28] Z. Liu, X. Zhang, Y. Mao, Y. Zhu, Z. Yang, C.T. Chan, P. Sheng, Locally resonant sonic materials, *Science*. 289 (2000) 1734-1736. https://science.sciencemag.org/content/289/5485/1734

[29] A. Qureshi, B. Li, K. Tan, Numerical investigation of band gaps in 3D printed cantilever-in-mass metamaterials, *Sci. Rep*. 6 (2016) 28314. https://www.ncbi.nlm.nih.gov/pmc/articles/PMC4916445/

[30] C.J. Naify, C.-M. Chang, G. McKnight, F. Scheulen, S. Nutt, Membrane-type metamaterials: Transmission loss of multi-celled arrays, *J. Appl. Phys.* 109 (2011) 104902. https://aip.scitation.org/doi/full/10.1063/1.3583656

[31] H. Zhang, Y. Xiao, J. Wen, D. Yu, X. Wen, Flexural wave band gaps in metamaterial beams with membrane-type resonators: theory and experiment, *J. Phys. D Appl. Phys.* 48 (2015) 435305.

https://iopscience.iop.org/article/10.1088/00223727/48/43/435305
[32] Y. Xiao, J. Wen, D. Yu, X. Wen, Flexural wave propagation in beams with periodically attached vibration absorbers: band-gap behavior and band formation mechanisms, *J. Sound. Vib.* 332 (2013) 867-893. https://www.sciencedirect.com/science/article/pii/S0022460X12007596
[33] E. Nobrega, F. Gautier, A. Pelat, J. Dos Santos, Vibration band gaps for elastic metamaterial rods using wave finite element method, *Mech. Syst. Signal. Pr.* 79 (2016) 192-202. https://www.sciencedirect.com/science/article/pii/S0888327016001102
[34] Y. Xiao, J. Wen, X. Wen, Longitudinal wave band gaps in metamaterial-based elastic rods containing multi-degree-of-freedom resonators, *New. J. Phys.* 14 (2012) 033042. https://iopscience.iop.org/article/10.1088/1367-2630/14/3/033042/meta
[35] H.-H. Huang, C.-K. Lin, K.-T. Tan, Attenuation of transverse waves by using a metamaterial beam with lateral local resonators, *Smart. Mater. Struct.* 25 (2016) 085027. https://iopscience.iop.org/article/10.1088/0964-1726/25/8/085027/meta
[36] D. Yu, Y. Liu, H. Zhao, G. Wang, J. Qiu, Flexural vibration band gaps in Euler-Bernoulli beams with locally resonant structures with two degrees of freedom, *Phys. Rev. B.* 73 (2006) 064301. https://journals.aps.org/prb/abstract/10.1103/PhysRevB.73.064301
[37] Y. Xiao, J. Wen, X. Wen, Flexural wave band gaps in locally resonant thin plates with periodically attached spring–mass resonators, *J. Phys. D Appl. Phys.* 45 (2012) 195401. https://iopscience.iop.org/article/10.1088/0022-3727/45/19/195401/meta
[38] Y. Li, L. Zhu, T. Chen, Plate-type elastic metamaterials for low-frequency broadband elastic wave attenuation, *Ultrasonics.* 73 (2017) 34-42. https://www.sciencedirect.com/science/article/pii/S0041624X16301524
[39] M. Nouh, O. Aldraihem, A. Baz, Wave propagation in metamaterial plates with periodic local resonances, *J. Sound. Vib.* 341 (2015) 53-73. https://www.sciencedirect.com/science/article/pii/S0022460X14010347
[40] G.L. Huang, C.T. Sun, Band Gaps in a Multiresonator Acoustic Metamaterial, *J. Sound. Vib.* 132 (2010) 031003-031003-031006. https://vibrationacoustics.asmedigitalcollection.asme.org/article.aspx?articleid=1471467
[41] Y. Chen, M. Barnhart, J. Chen, G. Hu, C. Sun, G. Huang, Dissipative elastic metamaterials for broadband wave mitigation at subwavelength scale, *Comp. Struct.* 136 (2016) 358-371. https://www.sciencedirect.com/science/article/pii/S0263822315008946

[42] P.F. Pai, H. Peng, S. Jiang, Acoustic metamaterial beams based on multi-frequency vibration absorbers, *Int. J. Mech. Sci.* 79 (2014) 195-205. https://www.sciencedirect.com/science/article/pii/S0020740313003482?via%3Dihub

[43] H. Peng, P.F. Pai, H. Deng, Acoustic multi-stopband metamaterial plates design for broadband elastic wave absorption and vibration suppression, *Int. J. Mech. Sci.* 103 (2015) 104-114. https://www.sciencedirect.com/science/article/pii/S0020740315003136

[44] X. Xiao, Z. He, E. Li, A. Cheng, Design multi-stopband laminate acoustic metamaterials for structural-acoustic coupled system, *Mech. Syst. Signal. Pr.* 115 (2019) 418-433. https://www.sciencedirect.com/science/article/pii/S0888327018303406

[45] E.J.P. Miranda, E.D. Nobrega, A.H.R. Ferreira, J.M.C. Dos Santos, Flexural wave band gaps in a multi-resonator elastic metamaterial plate using Kirchhoff-Love theory, *Mech. Syst. Signal. Pr.* 116 (2019) 480-504. https://www.sciencedirect.com/science/article/pii/S0888327018303959

[46] H. Sun, X. Du, P.F. Pai, Theory of metamaterial beams for broadband vibration absorption, *J. Intel. Mater. Syst. Struct.* 21 (2010) 1085-1101.

[47] P.F. Pai, Metamaterial-based broadband elastic wave absorber, *J. Intel. Mater. Syst. Struct.* 21 (2010) 517-528. https://journals.sagepub.com/doi/10.1177/1045389X10375637

[48] K.H. Matlack, A. Bauhofer, S. Krödel, A. Palermo, C. Daraio, Composite 3D-printed metastructures for low-frequency and broadband vibration absorption, *P. Natl. Acad. Sci.* 113 (2016) 8386-8390. https://www.pnas.org/content/113/30/8386

[49] F. Lucklum, M. Vellekoop, Design and Fabrication Challenges for Millimeter-Scale Three-Dimensional Phononic Crystals, *Crystals*. 7 (2017) 348. https://www.mdpi.com/2073-4352/7/11/348

[50] F. Lucklum, M.J. Vellekoop, Bandgap engineering of three-dimensional phononic crystals in a simple cubic lattice, *Appl. Phys. Lett.* 113 (2018) 201902. https://aip.scitation.org/doi/10.1063/1.5049663

[51] X. Zheng, W. Smith, J. Jackson, B. Moran, H. Cui, D. Chen, J. Ye, N. Fang, N. Rodriguez, T. Weisgraber, Multiscale metallic metamaterials, *Nat. Mater.* 15 (2016) 1100. https://www.nature.com/articles/nmat4694

[52] D. Beli, A.T. Fabro, M. Ruzzene, J.R.F. Arruda, Wave attenuation and trapping in 3D printed cantilever-in-mass metamaterials with spatially correlated variability, *Sci. Rep.* 9 (2019) 5617. https://www.nature.com/articles/s41598-019-41999-0

[53] A.T. Fabro, N.S. Ferguson, B.R. Mace, Wave propagation in slowly varying waveguides using a finite element approach, *J. Sound. Vib.* 442 (2019) 308–329. https://www.sciencedirect.com/science/article/pii/S0022460X18307569